

Observed Wind and SST Variability off the California Coast During Summertime High Wind Events

Weiguang Wu^{1,2}, Ana. B. Villas Bôas¹, and Sarah. T. Gille¹

¹Scripps Institution of Oceanography, University of California San Diego, La Jolla, CA, USA

²Now at MIT-WHOI Joint Program in Oceanography/Applied Ocean Sciences and Engineering,
Massachusetts Institute of Technology, Cambridge, MA, USA

Key Points:

- Wind events exceeding 9 m/s are a characteristic feature off the California coast in spring/summer.
- High wind events lead to sea surface temperature cooling at both nearshore and offshore buoy locations.
- The sea surface temperature response to wind events depends on the event duration and the strength of wind speed.

Corresponding author: Weiguang Wu, weiguang@mit.edu

Abstract

Sea surface winds off the California coast are characterized by high wind events that occur in spring and summer. In June, a well-defined wind event region is formed off the five major capes, extending ~ 300 km offshore. In the present work, a satellite wind product is used to study the spatial variability of these wind events. High-speed and long-duration events primarily occur off Cape Mendocino, whereas low-speed and short-duration events are more uniformly distributed over the wind event region. Coastal buoy observations show an anti-correlation between wind speed and sea surface temperature (SST) during wind events: a decrease in wind speed accompanies an increase in SST before the start of events, and an increase in wind speed accompanies a decrease in SST after the start of events. Different SST cooling patterns are observed within different categories of wind events: (1) High-speed events lead to more SST cooling compared to low-speed events. (2) Long-duration events lead to longer SST cooling times compared to short-duration events. SST cooling is observed both at nearshore buoy locations and at locations far from the coast. The magnitude of cooling is about 1°C nearshore and 0.3°C offshore. A case study of upper-ocean responses from mooring observations suggests that a combination of enhanced wind-driven mixing and Ekman pumping processes may explain SST cooling nearshore during wind events.

Plain Language Summary

Strong sea surface winds are a common phenomenon along the coast of California in summertime. The predominant northerly winds are intermittently interrupted by periods of weakening of wind speed caused by passing storms. These fluctuations lead to a series of high wind events occurring off the five major capes in spring and summer. In this study, we use a satellite wind product and coastal buoy observations to study these wind events. Wind events can be characterized based on their duration and the wind speed magnitude during the event. We find that both high-speed and long-duration events occur primarily off Cape Mendocino, whereas low-speed and short-duration events are more uniformly distributed over the wind event region. Buoy observations show that a decrease in wind speed corresponds to an increase in sea surface temperature (SST), while an increase in wind speed corresponds to a decrease in SST. SST cooling is observed both close to the coast and offshore, indicating that the cooling mechanism is not specific to the coastal regions. Based on a case study from ocean mooring observations, we hypothe-

size that a combination of enhanced wind-driven mixing and coastal upwelling processes are likely to explain SST cooling nearshore during wind events.

1 Introduction

Summertime winds off the California coast are primarily driven by a pressure gradient between the North Pacific High (NPH) and a thermal low over the southwest United States (Halliwell & Allen, 1987). This pressure gradient results in predominantly along-shore, upwelling-favorable winds that tend to cool the sea surface, reducing the thickness of the marine atmospheric boundary layer (MABL) (Koraćin & Dorman, 2001; Dorman et al., 2000, 2013). The alongshore flow in the MABL interacts with a series of capes along the California coast (see Figure 1), causing the wind to decelerate on the upwind side of the capes and accelerate on the downwind side, giving rise to a phenomenon known as “expansion fan” winds (Edwards et al., 2001; Koraćin et al., 2004).

The predominant northerly winds that are typical in spring and summer are intermittently interrupted by periods of weakening or even reversal caused by synoptic atmospheric systems. These fluctuations in the characteristic winds produce a cycle of alternating expansion fan winds and relaxation events. Fewings et al. (2016) proposed that these event cycles span about 12 days and that they happen in three stages: (1) Synoptic propagating cyclones weaken the predominant upwelling-favorable winds off Oregon/northern California. (2) After the cyclones propagate beyond the northward portion of the NPH, the NPH extends to the northeast, and the northerly wind intensifies along the coast of central California. (3) The northeast extension of the NPH advects warm desert air offshore, winds relax off the southern California coast, and the wind relaxation extends to northern California.

The question of how wind events impact SST variability in the California Current System (CCS) has been investigated in previous studies. The summer mean SST in the CCS is mainly the result of wind-driven coastal upwelling. Along the coast, positive wind-stress curl induces Ekman pumping, upwelling cold water toward the surface. This Ekman pumping increases during wind intensification and reduces during the wind relaxation stage (e.g. Taylor et al., 2008; Flynn et al., 2017). Besides the Ekman pumping mechanism, the net surface heat flux affected by the winds also contributes to SST variability in the three-stage wind cycle (Flynn et al., 2017). During stage 1 (wind relax-

77 ations), SST warming off the coast of Oregon/northern California is caused mostly by
78 reduced latent cooling due to weakened winds and by increased shortwave radiation due
79 to decreased cloudiness. However, the net heat flux is not the main driver of SST vari-
80 ability near the coast during stage 2 (wind intensification) and stage 3 (southern wind
81 relaxations), when changes in the rates of wind-driven mixing and Ekman pumping may
82 play major roles. Another possible mechanism that changes SST is horizontal advection.
83 The weakening or intensification of equatorward winds during wind events can lead to
84 increased warm poleward flow or cold equatorward flow in the ocean along the Califor-
85 nia coast (e.g. Send et al., 1987; Chelton et al., 1988; Melton et al., 2009). Moreover,
86 nonlinear effects become more important at smaller scales. The change of wind patterns
87 over a relatively short period of time may influence the rate of nonlinear Ekman pump-
88 ing through eddy-wind interactions (McGillicuddy et al., 2007) and may modify subme-
89 soscale SST frontal structures (Thomas & Lee, 2005).

90 Although some recent satellite-based studies have explored the evolution of wind
91 events and the corresponding upper-ocean response (e.g. Taylor et al., 2008; Melton et
92 al., 2009; Fewings et al., 2016; Flynn et al., 2017), the spatial variability of these events
93 and a more detailed characterization of their climatology remain unclear. Buoy-based
94 wind and SST measurements provide a consistent and long-enough temporal record that
95 allows us to further separate the wind events into different categories (e.g. long vs short,
96 strong vs weak) and to explore nuances of the SST response to these events. In the present
97 study, we first identify wind events based on wind speed and wind direction (section 2.4).
98 We then assess the spatial and seasonal evolution of these events in the CCS (section 3.1),
99 and characterize the statistics of different categories of wind events (section 3.2). In sec-
100 tion 3.3, we use buoy measurements to study SST variability within wind events, and
101 we explore the relationship between SST and the duration and strength of wind events
102 (section 3.4). Finally, in section 4, we explore possible mechanisms that could explain
103 wind/SST variability during these wind events.

104 **2 Data and Methods**

105 **2.1 CCMP Surface Ocean Vector Winds**

106 The Cross-Calibrated Multi-Platform (CCMP v2.0) gridded surface vector wind
107 dataset (Atlas et al., 2011; Mears et al., 2019) is an analysis product produced by Re-

108 mote Sensing Systems (RSS). CCMP v2.0 uses a variational analysis method to com-
109 bine version-7 of RSS radiometer wind speeds, QuikSCAT and ASCAT scatterometer
110 wind vectors, moored buoy wind measurements, and ERA-Interim model wind fields. The
111 final global product provides 6-hourly gap-free 10 m ocean vector winds, with a spatial
112 resolution of $0.25^\circ \times 0.25^\circ$ in latitude and longitude. It is available from 1987 to the present.
113 In this study, we use CCMP v2.0 6-hourly winds from 2002 to 2015 off the California
114 coast, in the region extending over 25° – 45° N and 110° – 140° W.

115 2.2 NDBC Buoy Measurements

116 To study the effects of high wind events on SST variability, we use meteorological
117 buoy measurements from the National Data Buoy Center (NDBC), which reports hourly
118 4-m wind speed with an accuracy of $\pm 1 \text{ m s}^{-1}$ and wind direction with an accuracy of
119 $\pm 10^\circ$. NDBC wind speeds are converted from 4 m to 10 m using a power law scaling (Hsu
120 et al., 1994). The NDBC buoys also provide hourly measurements of SST. Buoy tem-
121 perature sensors are located about 0.7 m below the water line and have an accuracy of
122 $\pm 1^\circ\text{C}$. For this study, six NDBC buoys in the CCS region are selected with record lengths
123 ranging from 18 to 32 years. The locations of these buoys are shown in Figure 1. Table 1
124 lists the geographic coordinates, time span, and distance to coast for each buoy. Since
125 diurnal variability is not the focus of this study, and the wind events that we study oc-
126 cur over time scales of days and weeks, a low-pass Hanning filter with cutoff frequency
127 of $(36 \text{ hr})^{-1}$ is applied to the 10-m wind speed and sea surface temperature time series.
128 We select data from April to July when wind events are prevalent (Figure 3). The low-
129 pass filtered data for each four-month spring segment are also detrended to remove the
130 seasonal trend.

131 2.3 CCE Mooring Measurements

132 A case study discussed in section 4 uses upper-ocean measurements from CCE-2
133 (e.g. Ohman et al., 2013; Martz et al., 2014), one of moorings of the California Current
134 Ecosystem (CCE) project. The mooring is located about 30 km southwest of Point Con-
135 ception, where the water depth is about 800 m (Figure 3). MicroCAT sensors on CCE2
136 measure water temperature and salinity every half hour at depths of 7 m, 15 m, 26 m,
137 46 m. Here we use measurements at these depths from the 3rd and 4th deployments of
138 CCE2 (CCE2-03/04) from March 2012 to May 2014. For each depth, we calculate the

139 potential temperature and density (referenced to 2000 m) using the TEOS-10 seawater
 140 toolbox (McDougall & Barker, 2011). For consistency, the data are low-pass filtered with
 141 a cutoff timescale of 36 hr.

142 **2.4 Definition of High Wind Events**

143 Previous studies have defined wind events in different ways. For example, Melton
 144 et al. (2009) identified the onset of southern wind relaxations by finding the zero cross-
 145 ings of the time amplitude for the first empirical orthogonal function of the 36 hr low-
 146 pass filtered along-principal-axis wind speed at four NDBC buoys near Pt. Conception,
 147 and they required the speed to exceed the mean at least 70% of the time for 3 days be-
 148 fore the onset and to be below the mean at least 60% of the time for 2.5 days after the
 149 onset. Fewings et al. (2016) and Flynn et al. (2017) adopted the definition from Melton
 150 et al. (2009) to study the 12-day evolution of the three-stage wind events and the SST
 151 response to these wind events. In contrast, Taylor et al. (2008) used NDBC buoy winds
 152 to define wind intensification events as occurring when the along-principal-axis wind speed
 153 exceeds the 75th percentile of the monthly wind distribution for at least 18 hrs over a
 154 35-hr period.

155 In this study, we relax these previous definitions to find high-speed wind events from
 156 April to July according to the following method: we fix the wind speed threshold to be
 157 9 m s^{-1} , which is the 90th percentile of CCMP wind speeds in June from 2002 to 2015
 158 within the study region (25° – 45° N and 110° – 140° W). This wind speed threshold is used
 159 for every grid point in the domain for any given month. Here we define a wind event as
 160 the time period when the wind speed exceeds the 9 m s^{-1} threshold with wind direction
 161 coming from 270° to 360° (with 360° representing northerly winds) for at least 36 hrs
 162 (6 consecutive CCMP data points). The start of a wind event occurs when the wind speed
 163 first exceeds the 9 m s^{-1} threshold. One such event occurred in May 2005 at 35.625° N,
 164 121.875° W (Figure 2a). The blue area of Figure 2a indicates the evolution of the event.

165 We apply the same wind event definition to the four near-shore NDBC buoys, 46014,
 166 46013, 46026, and 46028, except that we allow hourly wind speed to drop below 9 m s^{-1}
 167 threshold occasionally (less than 6 hrs) during the event. In Figure 2b, we show the NDBC
 168 buoy 46028 representation of the event in Figure 2a, with CCMP and buoy locations cho-
 169 sen to be as close as possible to each other spatially. The red area indicates the evolu-

170 tion of the event. CCMP suggests a slightly later start time than the buoy, which we at-
 171 tribute to the coarse temporal resolution of the CCMP wind product. Wind events ob-
 172 served by the buoys also show an overall higher wind speed than CCMP wind events.
 173 For the offshore buoys (46006 and 46059), where the summer wind speed is relatively
 174 weak (Figure 1), wind events are not a dominant phenomena during the spring and sum-
 175 mer, yet wind events with relatively high wind speed can still be observed. These events
 176 are likely associated with propagating storms. Since the wind direction is highly vari-
 177 able during high wind speed events at these off-shore locations, we impose no restriction
 178 on the wind direction but keep the 9 m s^{-1} wind speed threshold to identify the offshore
 179 high-wind events.

180 2.5 Composite Wind Speed/SST

181 To capture the mean evolution of wind events at a single buoy location, we con-
 182 struct composite means of wind speed and SST for every hour from 96 hrs before the
 183 onset of the event (negative lag) to 96 hrs after the onset (positive lag), making in to-
 184 tal a 193-hr time period, regardless of the duration of each individual event. To do this,
 185 we average wind speed/SST at every lag hr over all wind events to obtain the compos-
 186 ite mean of wind speed (blue lines, Figure 5,6) and SST (red lines, Figure 5,6). Events
 187 with missing data are not included in the analysis. There are 225 valid wind events for
 188 buoy 46014, 280 events for 46013, 141 events for 46012, 265 events for 46028, 158 events
 189 for 46006, 113 events for 46059. Uncertainties (shaded areas in Figures 5 and 6) corre-
 190 spond to one standard error of the mean of wind speed/SST at each lag hr.

191 3 Results

192 3.1 Spatial and Seasonal Variability of Wind Events

193 For every CCMP grid point in the region (28° – 43° N, 110° – 135° W), we find all wind
 194 events from 2002 to 2015 using the definition described in section 2.4. Then, we calcu-
 195 late the monthly cumulative duration by summing the duration of individual events that
 196 occurred in each month, and plot the average monthly cumulative duration of wind events
 197 between 2002 and 2015 (Figure 3). Thus, the “cumulative duration” at each location rep-
 198 represents the average number of days within a month when there are wind events. To show
 199 the seasonal variability of wind events, we also show the maps in fall and winter when

200 wind events are less common. Based on the June map when wind events are most com-
 201 mon, we define the “wind event region” to be where the average monthly cumulative du-
 202 ration exceeds 7 days (red contour line).

203 High winds off the California coast vary both spatially and seasonally, as shown
 204 in Figure 3. From November to January, the averaged cumulative duration per month
 205 (“cumulative duration”, hereinafter) is small: most of the wind events occur off Point
 206 Conception, with a cumulative duration less than 5 days. From February to March, wind
 207 events start to grow in the lees of Cape Mendocino and Point Conception with a cumu-
 208 lative duration of about 8 days, and an embryonic structure of expansion fan winds can
 209 be seen at these two major capes. The structure continues to grow and becomes well-
 210 developed in June from the California-Oregon border to southern California, extending
 211 roughly 300 km offshore. A clear expansion fan wind signature is revealed at the five ma-
 212 jor capes (from north to south): Cape Blanco, Cape Mendocino, Point Arena, Point Sur,
 213 and Point Conception. The average cumulative duration within the wind event region
 214 is about 7 days in April, 9 days in May, and 11 days in June. The maximum occurs off
 215 Cape Mendocino in June with a cumulative duration of about 17 days. After June, the
 216 cumulative duration of wind events decreases off Point Sur and Point Conception. The
 217 average cumulative duration per month within the wind event region drops to about 7
 218 days, while wind events off Cape Mendocino remain relatively common with cumulative
 219 duration exceeding 10 days. The cumulative duration gradually decays in fall; the av-
 220 erage cumulative duration within the region in September is about 4 days. From Septem-
 221 ber to November, the region of high cumulative duration off Cape Mendocino starts to
 222 disappear, while events off Point Conception start to become more common with cumu-
 223 lative duration between 3 and 5 days.

224 **3.2 Classifying Wind Events: Speed and Duration**

225 Although wind events are defined to have speeds greater than 9 m s^{-1} for at least
 226 36 hrs, the duration and wind speed maximum of each event vary substantially, with the
 227 longest event lasting over two weeks and the most extreme event having a maximum wind
 228 speed of $\sim 30 \text{ m s}^{-1}$. To better understand speed–duration statistics, we sort April–July,
 229 2002–2015 CCMP wind events into three categories based on the event duration and the
 230 magnitude of wind speed:

- 231 • **Low-speed vs high-speed.** Events are classified as “low-speed” if the 90th per-
232 centile of wind speeds during the event is less than 15 m s^{-1} , while for “high-speed”
233 events the 90th percentile of wind speeds exceeds 15 m s^{-1} ;
- 234 • **Short-duration vs long-duration.** Events are classified as “short-duration” if
235 the duration of the event is less than 72 hrs, while “long-duration” events last more
236 than 72 hrs;
- 237 • **Low-speed long-duration vs high-speed short-duration.** Events are clas-
238 sified as “low-speed long-duration” if the duration is greater than 72 hrs and the
239 90th percentile of wind speeds is less than 15 m s^{-1} , while “high-speed short-duration”
240 events last less than 72 hrs but have the 90th percentile of wind speeds greater
241 than 15 m s^{-1} .

242 Table 2 summarizes the statistics of the three categories of wind events. Within
243 the wind event region (outlined by the red contour, Figure 3), 64% of events have a du-
244 ration less than 72 hrs, and 36% have a duration greater than 72 hrs. While short-duration
245 events (< 72 hrs) occur more frequently than long-duration events (>72 hrs) from April
246 to July, long-duration events contribute more to the total wind-event time in the wind
247 event region: short-duration events account for 43% of total wind-event time, and long-
248 duration events account for 57%. The percentage of total wind-event time is the sum of
249 the duration time of the events of a given category, computed for CCMP grid points within
250 the wind-event region, divided by the sum of duration time of all events defined in sec-
251 tion 2.4 within the wind-event region. Despite differences in the definition of wind events,
252 our results are consistent with those of Taylor et al. (2008), who also found, using a point
253 buoy measurement (NDBC 46014), that long-duration events are less frequently occur-
254 ring but contribute more to the wind-event time.

255 For events with different wind-speed magnitudes, 90% of total wind-event time and
256 93% of the events correspond to low-speed events, with 90th percentile wind speeds less
257 than 15 m s^{-1} . Low-speed long-duration events comprise 32% of number of events and
258 49% of total wind-event time. In contrast, high-speed short-duration events account for
259 only 3% of events and 2% of total wind-event time. Following the same steps discussed
260 in section 3.1, in Figure 4 we show the spatial variability of cumulative duration of these
261 three wind-event categories. The maps are averaged from April to July between 2002
262 and 2015. Both low-speed and short-duration events (Figure 4a,b) are well distributed

263 along the wind event region, extending ~ 300 km off shore, whereas most high-speed and
 264 long-duration events (Figure 4d,e) occur off Cape Mendocino. Compared to low-speed
 265 events (Figure 4a), high-speed events (Figure 4d) are confined closer to the coast, and
 266 compared to other events categories, high-speed short-duration events (Figure 4f) have
 267 much less cumulative duration and occur mostly at Cape Blanco, Cape Mendocino, and
 268 Pt Arena.

269 **3.3 Evolution of Composite Wind Speed and Sea Surface Temperature**

270 To understand the evolution of wind speed and the SST response during the wind
 271 events, we focus on four nearshore NDBC buoys within the wind event region. The com-
 272 posite mean of wind speed (blue lines, Figure 5) shows that wind events follow a distinct
 273 evolution pattern. At negative lags, the composite wind speeds are below the 9 m s^{-1}
 274 threshold, with an average minimum speed of $6\text{--}7 \text{ m s}^{-1}$ occurring 17 to 20 hrs prior to
 275 the identified onset of the wind event. As the wind event starts (lag 0 hr), the wind speed
 276 increases rapidly and peaks between 24 and 28 hrs after wind onset, with the averaged
 277 maximum speed of $12\text{--}13.5 \text{ m s}^{-1}$ depending on the buoy location. In a period less than
 278 48 hrs, the composite wind speed increases $\sim 6 \text{ m s}^{-1}$. This pattern of anomalously low
 279 wind speed before the wind event and peak wind speeds occurring ~ 24 hrs after the start
 280 of the event is consistent with results of Taylor et al. (2008). After the peak, the wind
 281 speed gradually falls toward the 9 m s^{-1} threshold. This cycle of weakening, intensify-
 282 ing, and then weakening for winds during the 193-hr event composite is also consistent
 283 with results from Fewings et al. (2016), who revealed, from QuickSCAT observations,
 284 a similar three-stage cycle of wind events spanning about 12 days along the California
 285 coast in summertime.

286 The composite mean of SST (red lines, Figure 5) evolves in opposition to wind speed:
 287 at negative lags, composite SST gradually increases as wind speed decreases and peaks
 288 between lag -9 hr and -12 hr with maximum SST $10.5\text{--}12^\circ\text{C}$. Compared to SST at lag
 289 -96 hr, a $0.3\text{--}0.5^\circ\text{C}$ warming can be observed at four buoy locations. The maximum of
 290 SST lags the minimum of wind speed by about 8 hrs. As the wind speed steadily increases,
 291 SST decreases continuously until about lag +48 hr, about 24 hrs after the peak of wind
 292 speed. Among the four buoys, the largest 1.2°C cooling of SST (with respect to SST max-
 293 imum) occurs at buoy 46014, and the least cooling is 0.75°C at buoy 46012. After lag
 294 +48 hr, SST remains anomalously cold, except at buoy 46014 where a slight warming

295 trend is observed. A similar pattern of decreasing SST with increasing wind speed is also
 296 observed at two far offshore sites, buoy 46006 and 46059 (red lines, Figure 6) but with
 297 a smaller range of cooling (about 0.3°C at buoy 46006 and 0.4°C at buoy 46059) com-
 298 pared to cooling observed at the four nearshore buoys. At all six buoy sites, a decrease
 299 in wind speed typically corresponds to an increase in SST before the wind events start,
 300 and an increase in wind speed corresponds to a decrease in SST after the start of event.

301 **3.4 SST Response to Categories of Wind Events**

302 Overall, the temporal evolution of composite wind speed and SST is consistent across
 303 the four coastal buoys during the wind events. However, the relationship between wind
 304 speed and SST can be sensitive to wind-event duration and the magnitude of the wind
 305 speed. To investigate this relationship, based on the definition described in section 3.2,
 306 we classify NDBC wind events into three categories: (1) low-speed vs high-speed; (2) short-
 307 duration vs long-duration; (3) low-speed long-duration vs high-speed short-duration. For
 308 each scenario, the resulting composite mean wind speed (green dashed lines) and SST
 309 (orange dashed lines) at buoy 46014 are shown in Figure 7. These are compared with
 310 the average over all events for wind speed (blue solid lines) and SST (red solid lines).

311 Before the onset of a wind event, wind speed and SST (dashed lines) show consis-
 312 tent patterns in all cases: wind speed decreases, while SST increases. The maximum SST
 313 ($\sim 11^{\circ}\text{C}$) and the minimum wind speed ($\sim 7\text{ m s}^{-1}$) are similar to those obtained from
 314 averaging all events (solid lines). After the onset of an event, the evolution varies depend-
 315 ing on the category of event.

316 Wind speed anomalies appear anti-correlated with SST anomalies. For low-speed
 317 events (Figure 7a), the composite mean of wind speed (green dashed line) is lower than
 318 the mean from averaging all events (blue solid line), while the composite mean of SST
 319 (orange dashed line) is warmer than the all-event average (red solid line). For high-speed
 320 events (Figure 7d), the wind speed is greater than the all-event average, while SST is
 321 colder than the all-event average. Similar patterns emerge at the other three nearshore
 322 buoy locations (panels a and d in Figures S1–S3): lower wind speeds consistently cor-
 323 respond to higher SSTs and vice versa. This relationship is also identifiable when com-
 324 paring short-duration events to high-speed short-duration events (panels b and f in Fig-
 325 ures 7, S1–S3). The wind speed at all buoy locations peaks at about lag +24 hr, and SST

326 has a minimum between lag +36-48 hr, implying a 12-24 hr offset between the wind and
327 SST extrema. A higher wind speed maximum for high-speed short-duration events leads
328 to a lower SST minimum compared to the SST minimum for all short-duration events.
329 However, uncertainties are large compared with differences, and more wind events might
330 be needed to obtain a more robust result.

331 The duration of wind events also impacts the SST response. Both short-duration
332 and long-duration events (Figure 7b,e) at buoy 46014 show wind-speed evolution con-
333 sistent with the all-event average (blue solid line) until 24 hrs after the event starts. Af-
334 ter lag +24 hr, the wind speed for short-duration events weakens quickly, whereas the
335 wind speed for long-duration events sustains high speeds through the end of the com-
336 posite. The SST response (Figure 7e) reveals that at positive lags, long-duration events
337 lead to continuously SST cooling of about 1.5°C with respect to the SST maximum. The
338 pattern of longer wind duration responding to longer cooling time can also be seen at
339 the other three nearshore buoy locations (Figures S1e, S2e, S3e). At buoy 46014 (Fig-
340 ure 7b), the weakening of wind speed after lag +24 hr corresponds to the warming of SST
341 after lag +48 hr. At the other three buoy locations, SST warming occurs around lag +36
342 hr (Figures S1b, S2b, S3b). At the end of the composite, SST is finally restored roughly
343 to the initial value. A similar relationship between the duration of high wind speed and
344 the duration of SST cooling is also observed in panels c and f.

345 **4 Discussion: What Causes the Change in SST During Wind Events?**

346 Based on the three-stage wind events proposed by Fewings et al. (2016), we expect
347 the evolution of wind speed (blue lines, Figure 5) to be associated with a similar mech-
348 anism of wind expansions interrupted by summertime synoptic atmospheric forcing. At
349 the buoy sites, the anti-correlation between SST and wind speed during wind events (Fig-
350 ure 5) is consistent with the satellite-derived results of Flynn et al. (2017), who showed
351 that along the California coast positive SST anomalies follow wind relaxations, and neg-
352 ative SST anomalies follow wind intensification. It remains an open question whether
353 this SST variability is controlled by air-sea heat flux, Ekman transport, wind-induced
354 turbulent mixing, or horizontal advection of SST by ocean currents. Building on some
355 results from Flynn et al. (2017), we will use mooring observations to analyze a case study
356 of upper-ocean response to wind events and explore the mechanisms that could account
357 for the warming and cooling trend of SST.

358 During the warming phases, our composites show that the SST warms at negative
359 lags before the onset of the events (Figure 5) and in the case of short-duration events,
360 it warms again at positive lags toward the end of the wind event (Figure 7b,f). Flynn
361 et al. (2017) showed that changes in surface heat flux offshore are the main driver of SST
362 warming during wind relaxation events north of 37°N. As the wind speed decreases, the
363 latent cooling is reduced, and due to decreased cloudiness, shortwave radiation increases
364 and longwave radiation is reduced. However, surface heat fluxes offshore do not explain
365 SST warming in response to wind relaxation south of 37°N, where the reduction in short-
366 wave radiation, by increased cloudiness, offsets the reduced latent cooling. As suggested
367 by Flynn et al. (2017), changes in the rate of wind-driven mixing and horizontal advec-
368 tion may play more important roles in explaining the warming there. Additionally, the
369 rate of cold water upwelled as a result of Ekman transport is expected to reduce as the
370 alongshore wind speed decreases. For four of the nearshore buoys in this study, we ex-
371 pect that the reduced upwelling rate also contributes to the observed SST warming pat-
372 tern.

373 Similarly to the periods of SST warming, the changes in the rate of coastal upwelling
374 and wind-driven mixing can be important in driving SST cooling. As wind speed increases,
375 enhanced vertical shear strengthens the homogenization between warm sea surface and
376 cold water below, and enhanced wind-stress curl increases the rate of upwelling cold wa-
377 ter below. Both mechanisms can lead to surface cooling but would have different signa-
378 tures within the water column. To explore these two mechanisms, we look at the tem-
379 poral evolution of upper-ocean water temperature and density during two wind events
380 at the CCE-2 mooring (Figure 8). Both wind events lasted about 50 hrs, and the po-
381 tential temperature contour plots for both indicate that the near-surface temperature
382 cools after the wind event starts. Reanalysis fields from ERA-Interim at the mooring lo-
383 cation indicate that surface heat flux is not the main driver of SST cooling (not shown).
384 The potential temperature over depths evolves differently for the two events: In Figure 8a,
385 the temperature at depth 7-26m cools as the event starts and warms around lag +100
386 hr, whereas the temperature at depth 26-46m warms as the wind speed increases and
387 cools after lag +100 hr; In Figure 8b, the temperature over all depths cools continuously.
388 Similar to potential temperature, time series of potential density over a range of depths
389 suggest two distinct processes that could explain the cooling. In case a, the convergence
390 of potential density time series from different depths after the wind event starts (i.e. start-

391 ing around lag +20 hr) is consistent with wind-driven vertical mixing. As wind weak-
392 ens, the upper 50 m restratifies, and the potential density time series separate (after ~ 100
393 hours). In case b, the potential densities at 7m, 15m, and 26m merge quickly after the
394 wind event starts, indicating mixing, but the water does not homogenize to 46 m depth.
395 Instead the 7-26 m potential density evolves in parallel with the 46 m potential density.
396 The shoaling of potential density time series at all depths in the upper 50 m is consis-
397 tent with upwelling being the dominant process responsible for SST cooling. Indeed, Taylor
398 et al. (2008) suggest that the upwelling peaks about 48 hours after the start of the wind
399 events, which may also explain the sustained SST cooling after +48 hr lags during the
400 long-duration events (red lines, Figure 7c,e).

401 Another indicator of enhanced coastal upwelling during wind events comes from
402 the comparison of SST cooling at nearshore and far-offshore buoys. At the farthest off-
403 shore buoy 46006, 0.3°C cooling of SST (the difference between minimum and maximum
404 SST) can be observed during wind events (red line, Figure 6a). Among the four nearshore
405 buoys, low-speed events at buoy 46028 show the least SST cooling (0.6°C , red line, Fig-
406 ure S3a). The composite wind speed time series at buoy 46028 (blue line, Figure S3a)
407 has statistics similar to those at buoy 46006 (blue line, Figure 6a) with a mean of $\sim 10\text{ m s}^{-1}$
408 and a maximum of $\sim 12\text{ m s}^{-1}$. At these two locations, potential temperature and den-
409 sity profiles from an Argo float climatology (Roemmich & Gilson, 2009) also show a sim-
410 ilar stratification near the sea surface (Figure S4). This similarity in wind statistics and
411 sea surface stratification suggests that wind-driven mixing at the two locations would
412 induce a similar magnitude of SST cooling. The greater SST cooling observed at buoy
413 46028, compared to buoy 46006, suggests that other processes, besides wind-driven mix-
414 ing, also contribute to SST cooling nearshore. Thus, based on the observations from the
415 CCE-2 mooring and 46028 and 46006 buoys, we hypothesize that SST cooling during
416 wind events in nearshore locations result from a combination of enhanced wind-driven
417 mixing and coastal upwelling. Additional processes could also contribute to temperature
418 changes as the wind speed increases. This could include increased equatorward flow of
419 cold water or reduced poleward flow of warm water along the California coast. An ar-
420 ray of moorings with current and temperature measurements would be needed to quan-
421 tify the role of horizontal advection in explaining SST variability during the wind events.

422 The mechanisms described above focus on the impact of wind on SST. SST can
423 also affect wind. A number of studies have explored mechanisms by which wind accel-

424 erates over warmer SST and slows over cooler SST as a result of changes of surface sta-
425 bility, hydrostatic pressure gradients, and momentum transfer (e.g. Samelson et al., 2006;
426 Small et al., 2008). This suggests that warm SST anomalies before the start of the wind
427 event could contribute to subsequent wind speed increases. SST cold anomalies at pos-
428 itive lags may also play a role in explaining the decrease in wind speed about 24 hrs af-
429 ter the onset of wind events (Figure 5). A fully coupled ocean-atmosphere model for the
430 CCS would be needed to quantify the role of air-sea interaction during the wind events.

431 5 Conclusion

432 This study has explored spatial and seasonal variability of high wind events along
433 the California coast. Using gridded CCMP wind products, we have shown that most of
434 wind events in winter occur off Point Conception, with a cumulative duration of less than
435 5 days per month, and then grow off Cape Mendocino in early spring with a cumulative
436 duration of about 8 days per month. A well-developed wind event region is formed in
437 June off the five major capes along the west coast, extending ~ 300 km offshore. The av-
438 erage cumulative duration in the region is 11 days per month, and the maximum is about
439 17 days per month, occurring off Cape Mendocino. Within the wind event region, 7%
440 of wind events are high-speed, with the 90th percentile of wind speeds greater than 15 m s^{-1} .
441 Events lasting longer than 72 hours, classified as long-duration, account for 36% of events.
442 Both high-speed and long-duration events are likely to occur off Cape Mendocino, whereas
443 low-speed and short-duration events are more uniformly distributed over the wind event
444 region. After July, the cumulative duration of wind events decreases to less than 7 days
445 per month south of Point Conception. In northern California, off Cape Mendocino, wind
446 events remain relatively common with monthly cumulative duration exceeding 10 days,
447 and they start to disappear in fall. In winter, the wind events off Point Conception start
448 to become more common with cumulative duration between 3 and 5 days per month.

449 Composite time series of wind events have been constructed based on NDBC buoy
450 measurements. These composites show that decreases in wind speed accompany increases
451 in SST and vice versa. This pattern is consistent across all six buoys analyzed here. We
452 define wind events as starting when the speed first exceeds 9 m s^{-1} . Under this defini-
453 tion, SST peaks about 10 hrs before the start of the event, and wind speed peaks 24 hrs
454 after the start. During wind events, SST cools by $0.93 \pm 0.07^\circ\text{C}$ (from maximum to min-

imum temperature) averaged over the four nearshore buoys, and $0.33 \pm 0.10^\circ\text{C}$ for two far-offshore buoys.

SST cooling patterns are characterized based on the magnitude of the wind speed and the event duration. Strong wind events and long duration wind events can both lead to significant cooling nearshore. Compared to low-speed events, high-speed events lead to more SST cooling. Compared to short-duration events, long-duration events lead to longer SST cooling time. From the SST cooling comparison between nearshore and far-offshore buoy locations, and two cases of upper-ocean responses to wind events at the CCE-2 mooring, we hypothesize that a combination of enhanced wind-driven mixing and Ekman pumping processes are likely to explain SST cooling nearshore during wind events.

Our results have shed light on how the upper-ocean responds to high winds both nearshore and offshore. Although the mooring observations that we analyzed here provided some suggestions of mechanisms contributing to SST cooling, an array of upper-ocean and MBL measurements together with a fully coupled ocean-atmosphere model for the CCS would be necessary to distinguish the roles of surface heat flux, wind-driven mixing, horizontal advection, and Ekman pumping in explaining SST responses to wind events.

Acknowledgments

CCE-2 mooring data were collected by U. Send et al. at the Scripps Institution of Oceanography, funded by the US National Oceanic and Atmospheric Administration, and are accessible through the international OceanSITES program. The Argo float climatology data were collected and made freely available by the International Argo Program and the national programs that contribute to it. The Argo Program is part of the Global Ocean Observing System. This project was supported by NASA grants NNX16AH67G, 80NSSC19K0059, and 80NSSC20K1136. WW was partially funded by N000014-17-1-2390. ABVB was partially funded by NASA Earth and Space Science Fellowship award number 80NSSC17K0326.

Data Availability Statement

CCMP Version-2.0 vector wind analyses are produced by Remote Sensing Systems. Data are available at <http://www.remss.com/measurements/ccmp/>. CCE-2 03/04 data can be accessed at <https://dods.ndbc.noaa.gov/thredds/catalog/data/oceansites/>

Table 1. Station ID, position, depth, time span, and distance to the nearest coast for the selected NDBC buoys along the California coast as well as CCE-2 moorings.

Station ID	Latitude ($^{\circ}$ N)	Longitude ($^{\circ}$ W)	Time Span	Distance to Coast (km)
NDBC 46006	40.8	137.48	1983–2013	1090
NDBC 46059	37.98	130.0	1994–2012	540
NDBC 46014	39.22	123.97	1983–2014	20
NDBC 46013	38.23	123.32	1983–2014	20
NDBC 46012	37.36	122.88	1983–2014	20
NDBC 46028	35.74	121.89	1983–2014	40
CCE-2	34.32	120.82	2012–2014	30

485 DATA/CCE2/catalog.html, and NDBC buoy data are available at <https://dods.ndbc>
486 [.noaa.gov/thredds/catalog/data/stdmet/catalog.html](https://dods.ndbc.noaa.gov/thredds/catalog/data/stdmet/catalog.html). The Argo float climatol-
487 ogy data can be accessed at http://sio-argo.ucsd.edu/RG_Climatology.html.

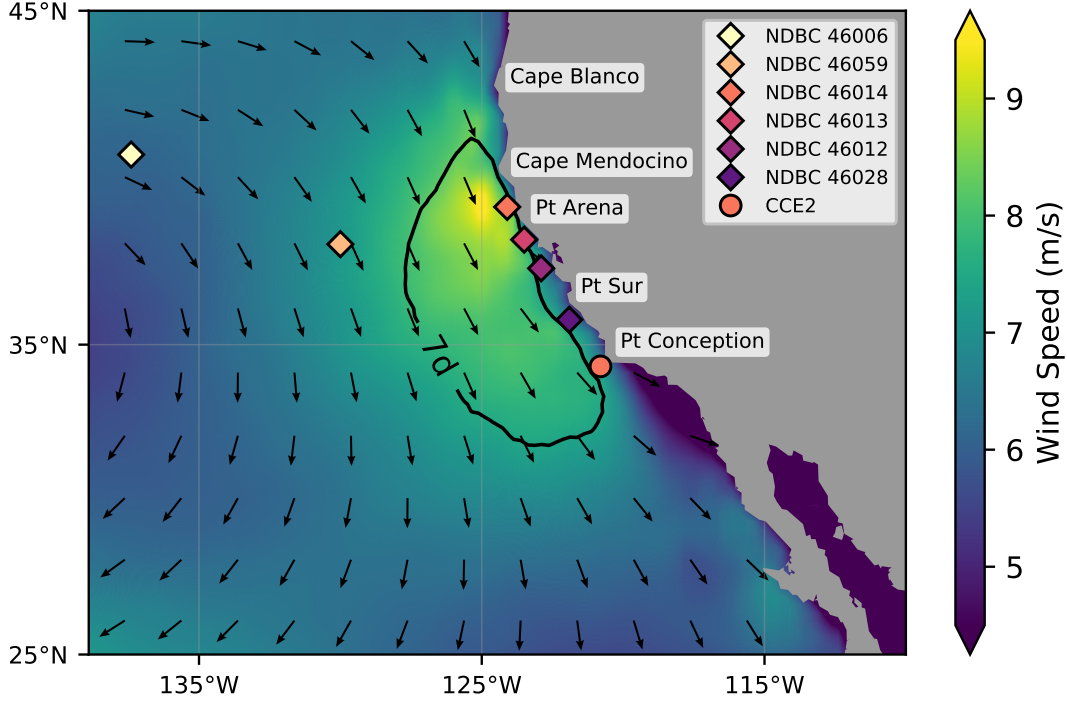


Figure 1. Average wind speed in June from CCMP reanalysis between 2002 to 2015. Colors indicate wind speed, and wind direction is shown as normalized vectors. The locations of six NDBC buoys and CCE-2 mooring, used in this study, are marked. The black contour line outlines the wind event region, which is defined in section 2.4.

Table 2. The percentage of number of events and the total wind-event time for different categories of wind events in the wind event region. The wind event region is outlined by the red contour in Figure 3. The percentage of number of events is the total number of the events of a given category divided by the total number of all events defined in section 2.4, computed for grid points within the wind event region. The percentage of total wind-event time is the sum time of the events of a given category divided by the sum time of all events within the wind event region. The definition for each type of wind events is in section 3.2.

Types of Wind Events	Percentage of Number of Events	Percentage of Total Event Time
Short-duration	64%	43%
Long-duration	36%	57%
Low-speed	93%	90%
High-speed	7%	10%
High-speed short-duration	3%	2%
Low-speed long-duration	32%	49%

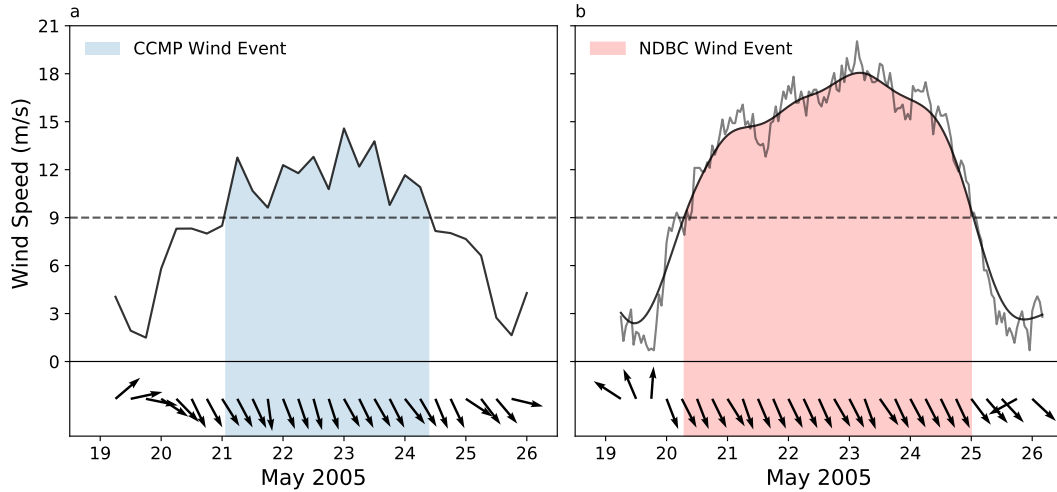


Figure 2. Example time series for a high wind event in May 2005 observed in two different datasets. (a) Time series of CCMP 6-hourly wind speed, along with corresponding wind direction (black arrows), at grid 35.625° N, 121.875° W. (b) Time series of NDBC hourly wind speed, along with the corresponding wind direction (black arrows) plotted at 6-hour spacing, of the same wind event identified at buoy, NDBC 46028 (35.7° N, 121.86° W), in May 2005. The gray line is the raw NDBC wind speed series. The black line is the filtered wind speed. The horizontal dashed line is the 9 m s^{-1} wind speed threshold. The shaded area represents the wind event.

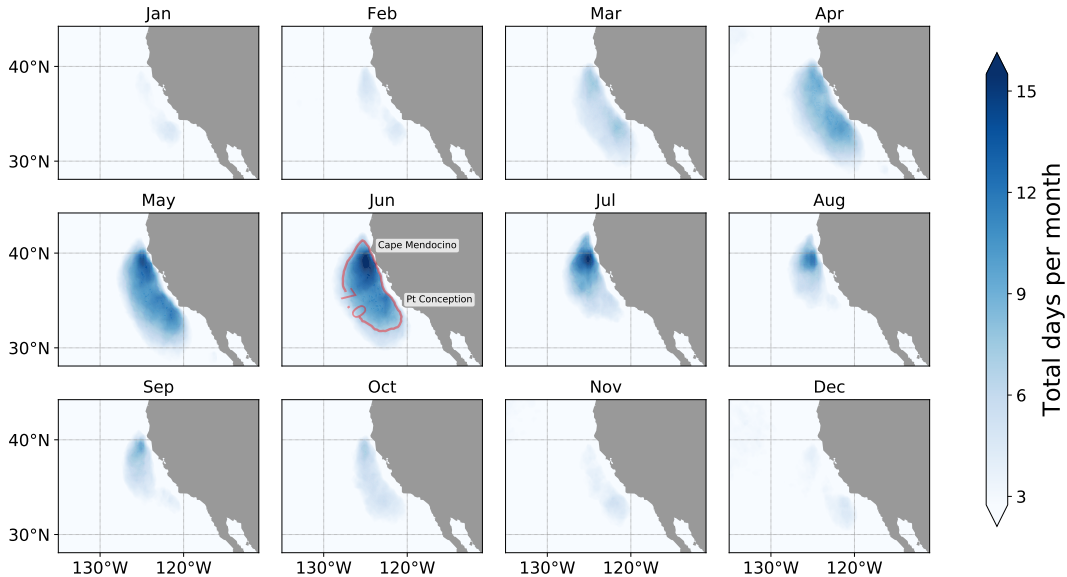


Figure 3. Maps of the average monthly cumulative duration of wind event from CCMP re-analysis between 2002 and 2015. The average cumulative duration (in units of total days per month) indicates the average number of days within a month when wind events occur. The contour of 7 days (red line) in the map of June outlines the wind event region.

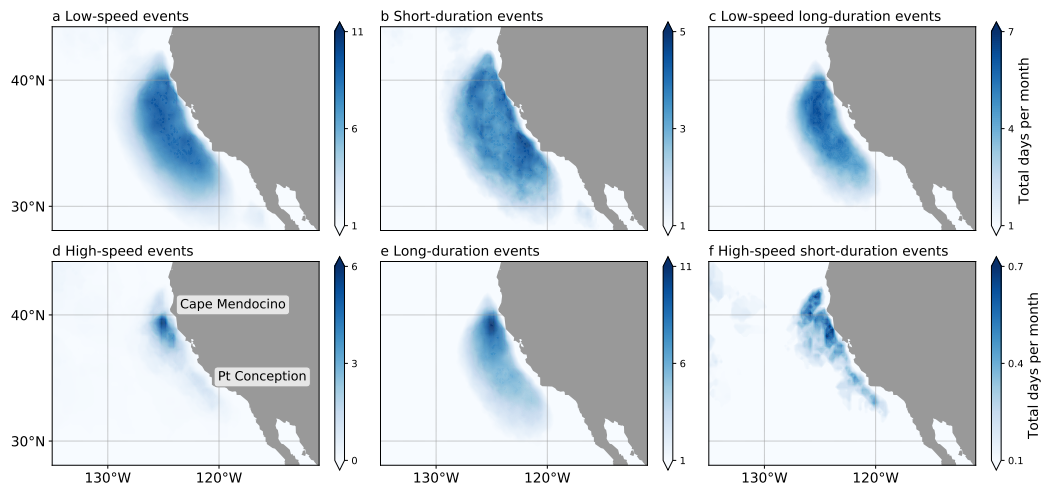


Figure 4. Maps of April-July average cumulative duration for (a) low-speed events, (b) short-duration events, (c) low-speed long-duration events, (d) high-speed events, (e) long-duration events, and (f) high-speed short-duration events. The classification of wind events is discussed in section 3.2. These events are identified from April to July between 2002 and 2015 based on CCMP wind vector reanalysis dataset. The average cumulative duration (in units of total days per month) indicates the average number of days within a month when wind events occur.

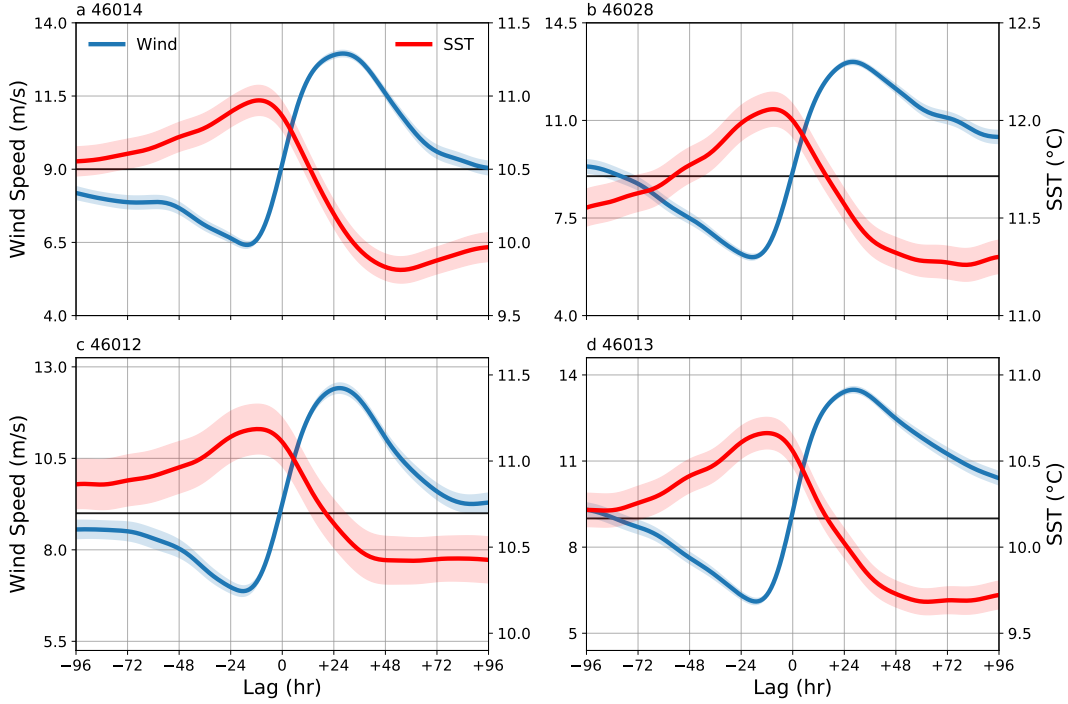


Figure 5. Evolution of composite mean of wind speed (blue lines) and SST (red lines) at four near-shore buoy locations. The composite is made from 96 hr before to 96 hr after the start of wind events. The horizontal black line indicates 9 m s^{-1} wind speed threshold for wind events. The composite mean at each lag hr is averaged over wind events selected from April to July between 1983 and 2014. Shaded areas correspond to one standard error of the mean for wind speed/SST at each lag hr. The number of events identified at 46014(a) is 225, at 46028(b) is 265, at 46012(c) is 141, at 46013(d) is 280. The mean of wind speed between lag -96 hr and 96 hr at 46014(a) is 9.2 m s^{-1} , at 46028(b) is 9.7 m s^{-1} , at 46012(c) is 9.3 m s^{-1} , at 46013(d) is 9.9 m s^{-1} . The mean of SST between lag -96 hr and 96 hr at 46014(a) is 10.4°C , at 46028(b) is 11.6°C , at 46012(c) is 10.8°C , at 46013(d) is 10.1°C .

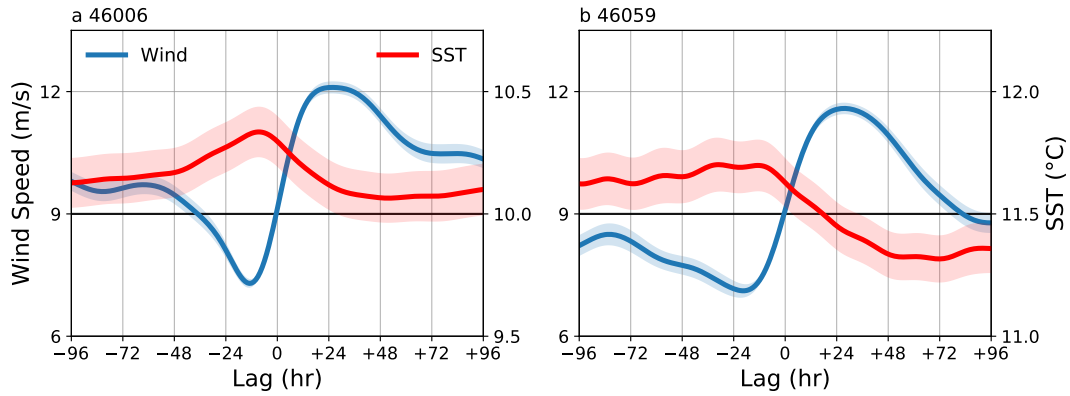


Figure 6. Evolution of composite mean of wind speed (blue lines) and SST (red lines) at two far off-shore buoy locations, where buoy 46006(a) is about 1000 km offshore and 46059(b) is about 500 km. The wind events at these two locations are selected with 9 m s^{-1} wind speed threshold without restriction on wind direction (see section 2.4 for details). The number of events identified at 46006 is 158, and at 46059 is 113. The mean of wind speed between lag -96 hr and 96 hr at 46006(a) is 10.0 m s^{-1} , and at 46059(b) is 9.1 m s^{-1} . The mean of SST between lag -96 hr and 96 hr at 46006(a) is 10.1°C , and at 46059(b) is 11.5°C .

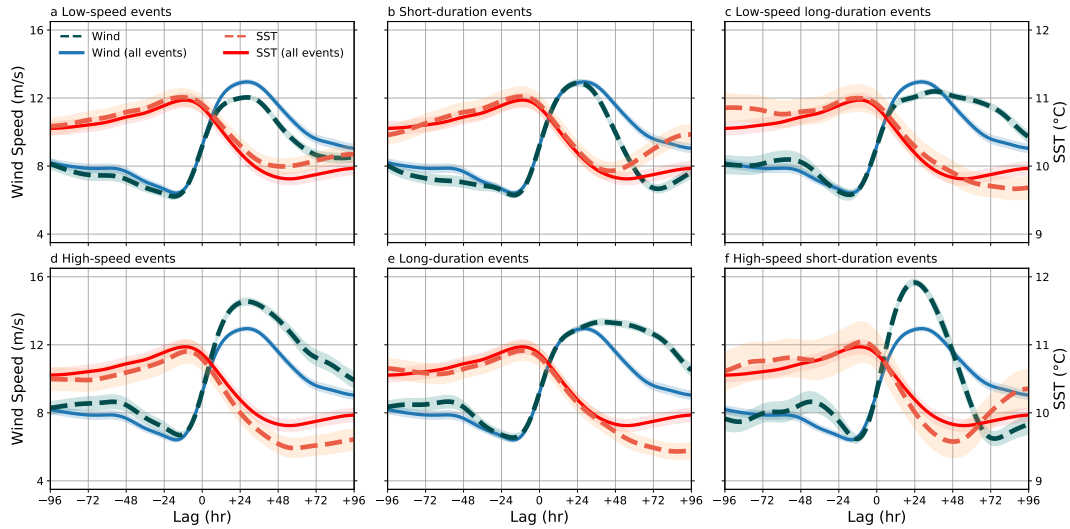


Figure 7. Evolution of composite mean of wind speed (green dashed lines) and SST (orange dashed lines) at buoy 46014 for (a) low-speed events, (b) short-duration events, (c) low-speed long-duration events, (d) high-speed events, (e) long-duration events, and (f) high-speed short-duration events. These events are identified from April to July between 1983 and 2014. Total number of events occurring at buoy 46014 is 225, and the number of events for each case is: 143(a), 115(b), 57(c), 82(d), 110(e), 29(f). The solid lines in each plot replicate the composite mean of SST (red) and wind speed (blue) over all 225 wind events at buoy 46014, shown in Figure 4a. Shaded areas correspond to one standard error of the mean for wind speed/SST at each lag hr.

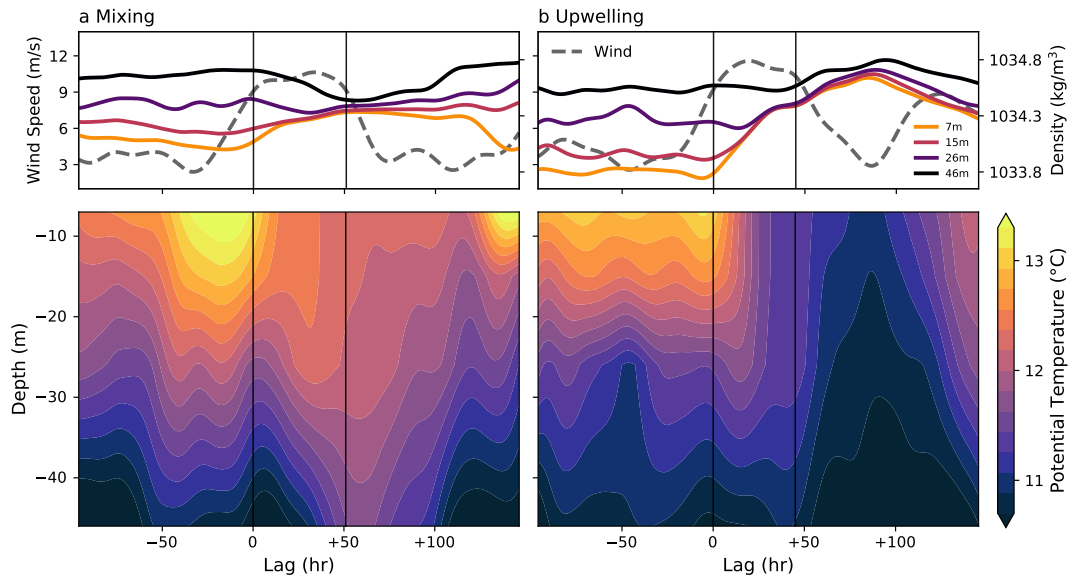


Figure 8. Time evolution of wind speed (dashed lines, upper panel), potential density at four depths (solid lines, upper panel), and potential temperature with depths (lower panel) for two wind events identified at CCE-2 mooring. (a) A wind event with a possible case of strong mixing, occurring in April 11, 2013, identified at CCE2-04. (b) A wind event with a possible case of enhanced upwelling, occurring in April 1, 2012, identified at CCE2-03. Vertical lines mark the onset and end time of the wind event.

488 **References**

- 489 Atlas, R., Hoffman, R. N., Ardizzone, J., Leidner, S. M., Jusem, J. C., Smith,
 490 D. K., & Gombos, D. (2011). A cross-calibrated, multiplatform ocean
 491 surface wind velocity product for meteorological and oceanographic appli-
 492 cations. *Bulletin of the American Meteorological Society*, *92*(2), 157–174.
 493 <https://doi.org/10.1175/2010BAMS2946.1>
- 494 Chelton, D. B., Bratkovich, A. W., Bernstein, R. L., & Kosro, P. M. (1988).
 495 Poleward flow off central California during the spring and summer of 1981
 496 and 1984. *Journal of Geophysical Research: Oceans*, *93*(C9), 10604–10620.
 497 <https://doi.org/10.1029/JC093iC09p10604>
- 498 Dorman, C. E., Holt, T., Rogers, D. P., & Edwards, K. (2000). Large-scale structure
 499 of the June–July 1996 marine boundary layer along California and Oregon.
 500 *Monthly Weather Review*, *128*(6), 1632–1652. [https://doi.org/10.1175/](https://doi.org/10.1175/1520-0493(2000)128<1632:LSS0TJ>2.0.CO;2)
 501 [1520-0493\(2000\)128<1632:LSS0TJ>2.0.CO;2](https://doi.org/10.1175/1520-0493(2000)128<1632:LSS0TJ>2.0.CO;2)
- 502 Dorman, C. E., Mejia, J. F., & Koraćin, D. (2013). Impact of U.S. west coastline
 503 inhomogeneity and synoptic forcing on winds, wind stress, and wind stress curl
 504 during upwelling season. *Journal of Geophysical Research: Oceans*, *118*(9),
 505 4036–4051. <https://doi.org/10.1002/jgrc.20282>
- 506 Edwards, K. A., Rogerson, A. M., Winant, C. D., & Rogers, D. P. (2001). Ad-
 507 justment of the marine atmospheric boundary layer to a coastal cape. *Journal*
 508 *of the Atmospheric Sciences*, *58*(12), 1511–1528. [https://doi.org/10.1175/](https://doi.org/10.1175/1520-0469(2001)058<1511:AOTMAB>2.0.CO;2)
 509 [1520-0469\(2001\)058<1511:AOTMAB>2.0.CO;2](https://doi.org/10.1175/1520-0469(2001)058<1511:AOTMAB>2.0.CO;2)
- 510 Fewings, M. R., Washburn, L., Dorman, C. E., Gotschalk, C., & Lombardo,
 511 K. (2016). Synoptic forcing of wind relaxations at Pt. Conception, Cal-
 512 ifornia. *Journal of Geophysical Research: Oceans*, *121*(8), 5711–5730.
 513 <https://doi.org/10.1002/2016JC011699>
- 514 Flynn, K. R., Fewings, M. R., Gotschalk, C., & Lombardo, K. (2017). Large-scale
 515 anomalies in sea-surface temperature and air-sea fluxes during wind relaxation
 516 events off the United States West Coast in summer. *Journal of Geophys-
 517 ical Research: Oceans*, *122*(3), 2574–2594. [https://doi.org/10.1002/](https://doi.org/10.1002/2016JC012613)
 518 [2016JC012613](https://doi.org/10.1002/2016JC012613)
- 519 Halliwell, G. R., & Allen, J. S. (1987). The large-scale coastal wind field along
 520 the west coast of North America, 1981–1982. *Journal of Geophysical Research:*

- 521 *Oceans*, 92(C2), 1861–1884. <https://doi.org/10.1029/JC092iC02p01861>
- 522 Hsu, S. A., Meindl, E. A., & Gilhousen, D. B. (1994). Determining the power-law
523 wind-profile exponent under near-neutral stability conditions at sea. *Jour-*
524 *nal of Applied Meteorology*, 33(6), 757–765. [https://doi.org/10.1175/](https://doi.org/10.1175/1520-0450(1994)033<0757:DTPLWP>2.0.CO;2)
525 [1520-0450\(1994\)033<0757:DTPLWP>2.0.CO;2](https://doi.org/10.1175/1520-0450(1994)033<0757:DTPLWP>2.0.CO;2)
- 526 Koračin, D., & Dorman, C. E. (2001). Marine atmospheric boundary layer diver-
527 gence and clouds along California in June 1996. *Monthly Weather Review*,
528 129(8), 2040–2056. [https://doi.org/10.1175/1520-0493\(2001\)129<2040:](https://doi.org/10.1175/1520-0493(2001)129<2040:MABLDA>2.0.CO;2)
529 [MABLDA>2.0.CO;2](https://doi.org/10.1175/1520-0493(2001)129<2040:MABLDA>2.0.CO;2)
- 530 Koračin, D., Dorman, C. E., & Dever, E. P. (2004). Coastal perturbations of
531 marine-layer winds, wind stress, and wind stress curl along California and Baja
532 California in June 1999. *Journal of Physical Oceanography*, 34(5), 1152–1173.
533 [https://doi.org/10.1175/1520-0485\(2004\)034<1152:CPOMWW>2.0.CO;2](https://doi.org/10.1175/1520-0485(2004)034<1152:CPOMWW>2.0.CO;2)
- 534 Martz, T., Send, U., Ohman, M. D., Takeshita, Y., Bresnahan, P., Kim, H.-J., &
535 Nam, S. H. (2014). Dynamic variability of biogeochemical ratios in the
536 Southern California Current System. *Geophysical Research Letters*, 41(7),
537 2496–2501. <https://doi.org/10.1002/2014GL059332>
- 538 McDougall, T. J., & Barker, P. M. (2011). *Getting started with TEOS-10 and*
539 *the Gibbs Seawater (GSW) Oceanographic Toolbox*. SCOR/IAPSO WG127.
540 http://www.teos-10.org/pubs/Getting_Started.pdf
- 541 McGillicuddy, D. J., Anderson, L. A., Bates, N. R., Bibby, T., Buesseler, K. O.,
542 Carlson, C. A., ... Steinberg, D. K. (2007). Eddy/wind interactions stimulate
543 extraordinary mid-ocean plankton blooms. *Science*, 316(5827), 1021–1026.
544 <https://doi.org/10.1126/science.1136256>
- 545 Mears, C. A., Scott, J., Wentz, F. J., Ricciardulli, L., Leidner, S. M., Hoffman,
546 R., & Atlas, R. (2019). A near-real-time version of the Cross-Calibrated
547 Multiplatform (CCMP) ocean surface wind velocity data set. *Journal of Geo-*
548 *physical Research: Oceans*, 124(10), 6997–7010. [https://doi.org/10.1029/](https://doi.org/10.1029/2019JC015367)
549 [2019JC015367](https://doi.org/10.1029/2019JC015367)
- 550 Melton, C., Washburn, L., & Gotschalk, C. (2009). Wind relaxations and
551 poleward flow events in a coastal upwelling system on the central Cal-
552 ifornia coast. *Journal of Geophysical Research: Oceans*, 114, C11016.
553 <https://doi.org/10.1029/2009JC005397>

- 554 Ohman, M. D., Rudnick, D. L., Chekalyuk, A., Davis, R. E., Feely, R. A., Kahru,
555 M., ... Send, U. (2013). Autonomous ocean measurements in the California
556 Current Ecosystem. *Oceanography*, *26*(3), 18–25. [https://doi.org/10.5670/
557 oceanog.2013.41](https://doi.org/10.5670/oceanog.2013.41)
- 558 Roemmich, D., & Gilson, J. (2009). The 2004–2008 mean and annual cycle of
559 temperature, salinity, and steric height in the global ocean from the Argo Pro-
560 gram. *Progress in Oceanography*, *82*(2), 81–100. [https://doi.org/10.1016/
561 j.pocean.2009.03.004](https://doi.org/10.1016/j.pocean.2009.03.004)
- 562 Samelson, R. M., Skillingstad, E. D., Chelton, D. B., Esbensen, S. K., O'Neill,
563 L. W., & Thum, N. (2006). On the coupling of wind stress and sea surface
564 temperature. *Journal of Climate*, *19*(8), 1557–1566. [https://doi.org/
565 10.1175/JCLI3682.1](https://doi.org/10.1175/JCLI3682.1)
- 566 Send, U., Beardsley, R. C., & Winant, C. D. (1987). Relaxation from upwelling
567 in the Coastal Ocean Dynamics Experiment. *Journal of Geophysical Research:
568 Oceans*, *92*(C2), 1683–1698. <https://doi.org/10.1029/JC092iC02p01683>
- 569 Small, R. J., deSzoeko, S. P., Xie, S.-P., O'Neill, L., Seo, H., Song, Q., ... Minobe,
570 S. (2008). Air–sea interaction over ocean fronts and eddies. *Dynamics of
571 Atmospheres and Oceans*, *45*(3-4), 274–319. [https://doi.org/10.1016/
572 j.dynatmoce.2008.01.001](https://doi.org/10.1016/j.dynatmoce.2008.01.001)
- 573 Taylor, S. V., Cayan, D. R., Graham, N. E., & Georgakakos, K. P. (2008).
574 Northerly surface winds over the eastern North Pacific Ocean in spring and
575 summer. *Journal of Geophysical Research: Atmospheres*, *113*, D02110.
576 <https://doi.org/10.1029/2006JD008053>
- 577 Thomas, L. N., & Lee, C. M. (2005). Intensification of ocean fronts by down-front
578 winds. *Journal of Physical Oceanography*, *35*(6), 1086–1102. [https://doi
579 .org/10.1175/JP02737.1](https://doi.org/10.1175/JP02737.1)